

Anisotropic Interlayer Exciton in GeSe/SnS van der Waals Heterostructure

Nikhilesh Maity, Pooja Srivastava, Himani Mishra, Ravindra Shinde, and Abhishek Kumar Singh*



Cite This: *J. Phys. Chem. Lett.* 2021, 12, 1765–1771



Read Online

ACCESS |



Metrics & More

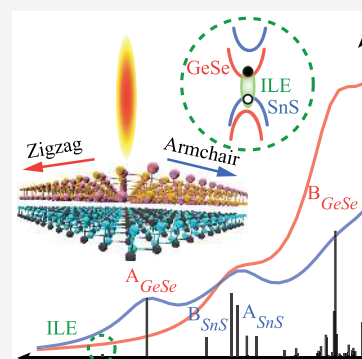


Article Recommendations



Supporting Information

ABSTRACT: Stacking two or more two-dimensional materials to form a heterostructure is becoming the most effective way to generate new functionalities for specific applications. Herein, using GW and Bethe–Salpeter equation simulations, we demonstrate the generation of linearly polarized, anisotropic intra- and interlayer excitonic bound states in the transition metal monochalcogenide (TMC) GeSe/SnS van der Waals heterostructure. The puckered structure of TMC results in the directional anisotropy in band structure and in the excitonic bound state. Upon the application of compressive/tensile biaxial strain dramatic variation ($\mp 3\%$) in excitonic energies, the indirect-to-direct semiconductor transition and the red/blue shift of the optical absorption spectrum are observed. The variations in excitonic energies and optical band gap have been attributed to the change in effective dielectric constant and band dispersion upon the application of biaxial strain. The generation and control over the interlayer excitonic energies can find applications in optoelectronics and optical quantum computers and as a gain medium in lasers.



The past decade has witnessed a growing interest in two-dimensional (2D) transition-metal dichalcogenides (TMDC) because of their prospects for electronics,^{1,2} spin/valley electronics,^{3,4} optoelectronics,^{5,6} and catalytic applications.⁷ Advances in experimental techniques have now made it possible to manipulate the properties of these 2D materials by stacking them together to generate a new kind of system called the van der Waals (vdW) heterostructure.^{8–10} The vdW heterostructure not only preserves the properties of monolayers, but quantum coupling between monolayers also provides a platform to play with the electronic and optical properties of these structures.^{11–13} For example, the heterostructure of semimetallic graphene and insulating h-BN acting as a vertical transport barrier exhibit a room temperature high ON/OFF ($>10^5$) switching ratio.¹⁴

Recently, the observation of interlayer excitons (ILE),^{15–18} where the electron and hole are confined in different layers, in TMDC/TMDC vdW type II heterostructures ignited a new interest in studying the optical properties of these 2D semiconducting materials. Because of the localization of electrons and holes in different layers, the spatially indirect or interlayer exciton possesses a relatively longer life span¹⁵ and shorter binding energies, which makes them fascinating for realizing the Bose–Einstein condensates¹⁹ and their applications in solar cells²⁰ and photodetectors.²¹ However, the high symmetry of the TMDC crystal makes the optical properties as well as the intensity of intra- and interlayer excitons directionally isotropic.^{11,16} In addition, the intensity of these excitons is insensitive to the nature of polarization of the incident light.

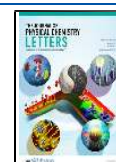
More recently, transition metal monochalcogenides (TMC), another class of 2D materials with structural anisotropy, have drawn the attention of the scientific community due to the presence of the anisotropic optical response and excitons. Anisotropic intralayer excitonic bound states are observed in the low-symmetric 2D layers of phosphorene,²² ReS₂,^{23,24} and monolayer TMC.^{25–27} These anisotropic properties can be further enhanced or tuned by making 2D TMC/TMC vdW heterostructures.

Here, using first-principles GW and Bethe–Salpeter equation (BSE) simulations, we report anisotropic IL excitonic bound states in the type II vdW heterostructure of TMCs GeSe/SnS. Interestingly, the optically active anisotropic inter- and intralayer excitons are linearly polarized along the armchair and zigzag directions, respectively. A direct correlation between the in-plane biaxial strain and band alignment is observed for the GeSe/SnS vdW heterostructure. On application of more than 1% strain, the linearly polarized anisotropic ILE disappeared because of the change in band alignment of the heterostructure. The effects of strain engineering are also observed on the peak position and binding energies of intra- and interlayer excitons.

Received: November 22, 2020

Accepted: February 8, 2021

Published: February 11, 2021



The computational methodology used in this present study has been discussed in detail in the [Supporting Information](#) (section 1). The stable α phase²⁸ of both monolayers, GeSe and SnS (space group $Pmn2_1$), with puckered and anisotropic structures are considered for this study. The convergence tests of ground state energy and optical absorption are performed and presented in [Figures S1–S5](#). The structures of individual layers ([Figure S6](#)) and their electronic, transport, and optical properties are discussed in detail in the [Supporting Information](#). These findings are in excellent agreement with previous reports.^{25–27} The GeSe/SnS heterostructure is constructed by stacking the optimized unit cells of individual monolayer TMCs, as shown in [Figure 1a,b](#) and [Figure S7](#). The

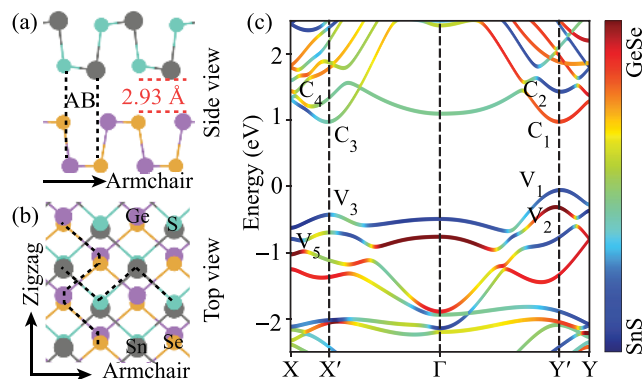


Figure 1. (a) Side view and (b) top view of the atomic structure of the GeSe/SnS heterostructure. The armchair and zigzag directions are indicated in (b). (c) Band structure of the GeSe/SnS heterostructure within the GGA-PBE approximation. The color gradient map reveals the projection of bands into the isolated monolayers.

lattice parameters (a , b) and interlayer distances (d) of the heterostructure with stacking AA and AB have been optimized ([Figure S7a–f](#)). The optimized lattice parameters for the more stable heterostructure with AB stacking are summarized in [Table S1](#).

The electronic band structure of the heterostructure calculated by using the GGA-PBE method is shown in [Figure 1c](#). The high symmetric directions Γ – Y and Γ – X in the reciprocal space represent the ac and zz directions, respectively, in the real space ([Figure 1c](#) and [Figure S8](#)). The GeSe/SnS heterostructure is found to be an indirect band gap semiconductor with a band gap value of 1.03 eV (1.56 eV) at the GGA-PBE (GW) level ([Figure S9](#)) of approximation ([Table S1](#)). The valence band maximum (VBM) and the conduction band minimum (CBM) are located at Y' and X' points, respectively. Interestingly, a competing minima in conduction band is observed at Y' in the GeSe/SnS heterostructure, which is almost degenerate with minima at X' (energy difference <0.1 eV). The direct semiconducting gaps at X' and Y' points are 1.95 and 1.64 eV ([Figure S9](#)), respectively. We observed a type II band alignment of the GeSe/SnS heterostructure at Y' (ac direction) in BZ. The conduction band at Y' (C_1) and the valence band at Y' (V_1) originate from the Ge- p_y state of the GeSe layer and Sn- s and S- p_y states of the SnS layer, respectively.

The structural anisotropy is reflected in band dispersion also; the conduction band is more dispersive along the Γ – X (zz) direction compared to the Γ – Y (ac) direction ([Figure 1c](#)). The nature of band dispersion of the valence band is opposite to that of the conduction band, where the valence

band is flat along the Γ – X (zz) direction compared to the Γ – Y (ac) direction. Because of the inverse proportionality between the effective mass and the curvature of the band dispersion, the effective mass of charge carriers ([Table S2](#)) and therefore the charge transport will also be anisotropic. For the heterostructure, calculated electron mobilities along the ac and zz directions are 7.55 and $18.00 \times 10^3 \text{ cm}^2 \text{ V}^{-1} \text{ s}^{-1}$, respectively. On the other hand, the hole mobilities along ac and zz are found to be 0.38 and $1.12 \times 10^3 \text{ cm}^2 \text{ V}^{-1} \text{ s}^{-1}$, respectively. Therefore, the electron mobility is 2.38 times and the hole mobility 2.95 times larger along the zz direction than that along the ac direction. The anisotropic transport properties can be attributed to the anisotropic geometrical structure of the TMCs as discussed earlier. Interestingly, the carrier mobility of the GeSe/SnS heterostructure is much higher than that in individual TMDs²⁹ and comparable to that of phosphorene.³⁰

To understand the optical behavior of the GeSe/SnS heterostructure, the optical absorption spectrum is calculated by using many-body perturbation theory in the GW+BSE approximation. The BSE for the excitonic state S of the wave function ψ_{cv}^S and energy E_S can be written as

$$(E_c^{\text{QP}} - E_v^{\text{QP}})|\psi_{cv}^S\rangle + \sum_{c'v'} K_{cv,c'v'}^{\text{eh}}|\psi_{c'v'}^S\rangle = E_S|\psi_{cv}^S\rangle \quad (1)$$

where $K_{cv,c'v'}^{\text{eh}}$ is the kernel of electron–hole interactions. The macroscopic dielectric function by BSE in the frequency domain of the system can be obtained from the expression

$$\text{Im}[\epsilon_{\text{BSE}}(\omega)] = \frac{16\pi e^2}{\omega^2} \sum_S |\langle 0|\mathbf{A} \cdot \mathbf{u}|\psi_{cv}^S\rangle|^2 \delta(E_S - \omega) \quad (2)$$

where \mathbf{u} is the velocity operator between valence and conduction energy state and \mathbf{A} is the polarization vector. Using the many-body perturbation theory in the GW approximation, we evaluate the optical absorption spectrum of GeSe/SnS heterostructure ([Figure 2a](#)). The solid and dashed lines correspond to the optical absorption of the heterostructure with (w/eh) and without electron–hole pair (wo/eh) interactions. Similar to the electronic properties, a profoundly distinct optical response of the heterostructure is obtained along the ac and zz directions. The optical absorption spectra calculated wo/eh interactions give the information on the quasi-particle band gaps of the heterostructure. The band edge is defined as the position where the increase in the rate of absorption (wo/eh interaction) is largest.²² The optical absorption spectrum of wo/eh of the ac and zz components yields the values of 1.64 and 1.95 eV, corresponding to the direct band gap values at Y' (representing ac) and X' (representing zz), respectively.

The excitonic effects are observed, when the e–h interactions are included in the optical absorption by the GW-BSE approximation. The four intense intralayer excitonic bound states corresponding to the individual monolayers of A_{GeSe} , B_{SnS} , A_{SnS} , and B_{GeSe} are also observed in the GeSe/SnS heterostructure. The intralayer excitons, localized along the ac and zz directions, are named as A and B excitons, respectively. The peak positions of the corresponding excitons are at 1.53, 1.79, 1.81, and 2.11 eV, respectively. The red shift of the peak positions of the intralayer excitons has been observed ([Figure S10a,b](#)) in heterostructure compared to the isolated monolayers. These changes in the heterostructure can be attributed

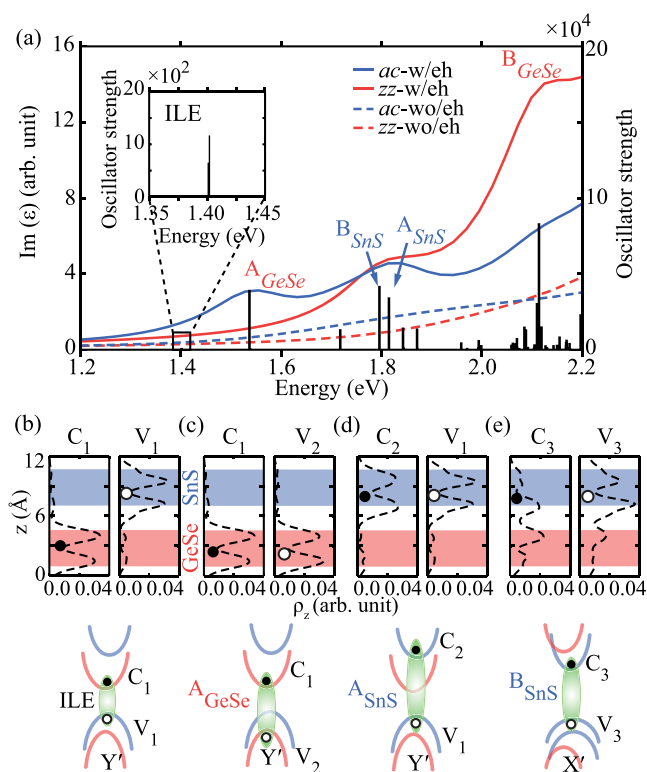


Figure 2. (a) Optical absorption spectra of the GeSe/SnS heterostructure calculated by using BSE (w/eh) and RPA (wo/eh) methods along the *zz* and *ac* directions. The vertical black lines represent the oscillator strength. The inset shows the calculated oscillator strength of the ILE. (b–e) Planar average charge density of the heterostructure along the *z*-direction and a schematic representation of intra- and interlayer excitonic bound states of the GeSe/SnS heterostructure.

to an increase in dielectric screening (Table S3). The puckered structure of this heterostructure results in the anisotropic optical response and the linearly polarized excitons in the system. The exciton binding energies, the difference between the electronic band gap and the optical band gap, E_{ex} of A_{GeSe} , A_{SnS} , B_{SnS} , and B_{GeSe} excitons are 0.19, 0.27, 0.15, and 0.68 eV, respectively. The binding energies of both intralayer A excitons are higher compared to that of B excitons (except B_{GeSe}). This implies that the excitonic bound states, which are localized along the *ac* direction, are more strongly bound compared to the *zz* direction. As discussed earlier, the carriers are more mobile along *zz* than that along the *ac* direction, which makes Coulomb interactions between electrons and holes weaker along the *zz* direction.

Apart from the linearly polarized intralayer bound states, an additional lowest energy transition state has been observed in the optical absorption spectrum along the *ac* direction below the A_{GeSe} by 0.14 eV (Figure 2a). This lowest energy state has been identified as the ILE, where electrons and holes reside on the GeSe and SnS layers, respectively. The ILE transition state is linearly polarized along the *ac* direction and appears due to the type II band alignment along this direction (at Y') as shown in Figure 1c. The value of binding energy of the ILE is 0.23 eV. In spite of the higher effective mass of the charge carriers along the *ac* direction, the ILE is weakly bound, which is due to the longer charge separation between the carriers leading to reduction in the effective Coulomb interactions between the e–h pairs. As a consequence of the charge

localization in different layers, the transition probability, which is given by the oscillator strength, is very low for the IL transition as shown in the inset of Figure 2a. Bader charge analysis indicates a charge transfer of $0.018e$ between the monolayers. This leads to a built-in electric field at the interface of the GeSe/SnS heterostructure, helping to separate electrons and holes in the different layers, leading to an increase in the recombination lifetime of the ILE. Our calculations predict that the ILE in GeSe/SnS is weakly coupled compared to that in the TMDC/TMDC heterostructures,^{16,18} which will help in the easier charge separation. Hence, the presence of the long recombination time and the weakly bound linearly polarized IL excitonic bound state can make the GeSe/SnS vdW heterostructure a potential candidate for photocatalysis and solar cell applications. Along with the excitons in this heterostructure, the biexcitons or multiexcitons can also play a role in light–matter interactions. However, the contribution of biexcitons and multiexcitons is negligible in comparison to excitonic effects in a 2D system. Furthermore, these higher order many-body effects arising due to the interaction of exciton–exciton or exciton–electron/hole cannot be captured by using BSE approximation.

A clear picture of localization of excitons emerges from the *z*-direction planar averaged charge density (Figure 2b–e) of heterostructure. The planar averaged charge density indicates that C_1 and V_1 originate from the GeSe and SnS layers, respectively (Figure 2b). Therefore, the ILE along the *ac* direction with very low oscillator strength originates from the interlayer excitonic transition from V_1 to C_1 at the Y' point as shown in Figure 2b. The C_1 and V_2 bands at the Y' point mainly originate from the GeSe layer. Therefore, A_{GeSe} exciton is formed by localization of electrons and holes in C_1 and V_2 at the Y' point, respectively (Figure 2c), whereas the C_2 and V_1 bands at the Y' point originate from the SnS layer (Figure 2d), which leads to the formation of A_{SnS} in the heterostructure. Figure 2e shows that B_{SnS} originates from the X' point, where C_3 and V_3 points mainly localized at the SnS layer. The low-energy optical active transitions are mostly dominated by the *ac* directional polarized excitons. Hence, GeSe/SnS heterostructure strongly absorbs *ac* polarized light in the energy range 1.40 eV (ILE peak position) to 1.80 eV and remains transparent to *zz* polarized light. Because of this unique anisotropic phenomenon, the heterostructure can be used as an optical polarizer²² and, in optical quantum computers, as three-dimensional visual displays and liquid crystal displays.^{31,32}

There is a chance to further enhance or modulate these properties by applying in-plane to the heterostructure. Previous reports also suggest that strain can tune the band gap as well as electronic and optical properties of 2D materials.^{33–39} The application of strain can also modulate the excitonic binding energies of a system by weakening or strengthening the dielectric screening of the medium.^{40,41} The applied uniaxial strains along the *x* (*zz*) and *y* (*ac*) directions are defined as $\epsilon_{zz} = \frac{a - a_0}{a_0}$ and $\epsilon_{ac} = \frac{b - b_0}{b_0}$. The complete relaxation along the *z* direction has been considered along with applied in-plane uniaxial and biaxial strains in the heterostructure. Structural change in the GeSe/SnS heterostructure is more sensitive to biaxial strains compared to the uniaxial strains (see Figure S7f). The BT stretched and BC compressed cell parameter strains are taken to be negative and positive values, respectively. Furthermore, the out-of-plane compressive and tensile strains

are also applied in the system to investigate the modulation of optical properties (detailed discussion in section 7 of the Supporting Information).

The evolution of the band edges (C_1 , V_1 , C_3 , and V_3) of the heterostructure with ϵ_{bi} is shown in Figure 3a. The indirect-to-

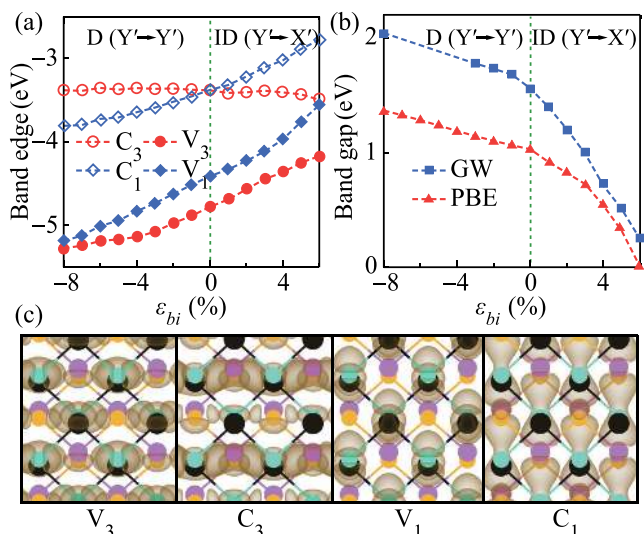


Figure 3. (a) Evolution of different band edges at X' and Y' as a function of ϵ_{bi} . (b) Variation of band gap values by GGA-PBE and GW methods with ϵ_{bi} . (c) Top view of band-decomposed charge density of different band edges at X' and Y' points, showing the bonding (C_3) and antibonding (V_3 , V_1 , and C_1 edges) character of the orbitals.

direct band gap transition has been observed upon application of ϵ_{bi} ($\approx -1\%$) (Figure 3a). Furthermore, under the application of ϵ_{bi} , the band gap of the system decreases continuously and becomes zero at 6% strain as shown in Figure 3b. Both of the transitions are due to the downward shift of the C_3 valley with ϵ_{bi} as shown in Figure 3a. The band-decomposed charge densities of VBM and CBM at both X' and Y' points are given in Figure 3c. The C_1 , V_1 , and V_3 valleys clearly show the antibonding character of the orbitals, whereas the C_3 valley shows the bonding characters of the orbitals. Upon application of compressive ϵ_{bi} on the unit cell, the atoms come closer to each other, and their wave functions start to overlap. As a result, the bonding nature of C_3 increases with the BC strain, leading to a downward shift of the C_3 point. On the other hand, with the BC strain the bonding nature of C_1 , V_1 , and V_3 points decreases, leading to a shift toward higher energy regions (Figure 3a).

The absorption spectrum shows a significant blue (red) shift with the applied BT (BC) strains with respect to the unstrained peak position as shown in Figure 4a–c (Figure 4d–f). The linearly polarized state of all the intralayer excitons has been preserved even under the strain in the system. On the other hand, the ILE is absent under high BC strain, $\epsilon_{bi} > 1\%$ (Figure 4f). First peak of the optical absorption (w/eh) determines the optical band gap of the system. Therefore, the optical band gap up to 1% strain is represented by peak position of the ILE and beyond that (Figure 4f) by the peak position of A_{GeSe} exciton. The shift in excitonic energies with biaxial in-plane (intra- and interlayer excitons) is shown as in Figure 4g. For out-of-plane strain, the absorption spectrum shows a red (blue) shift with tensile (compressive) strains with

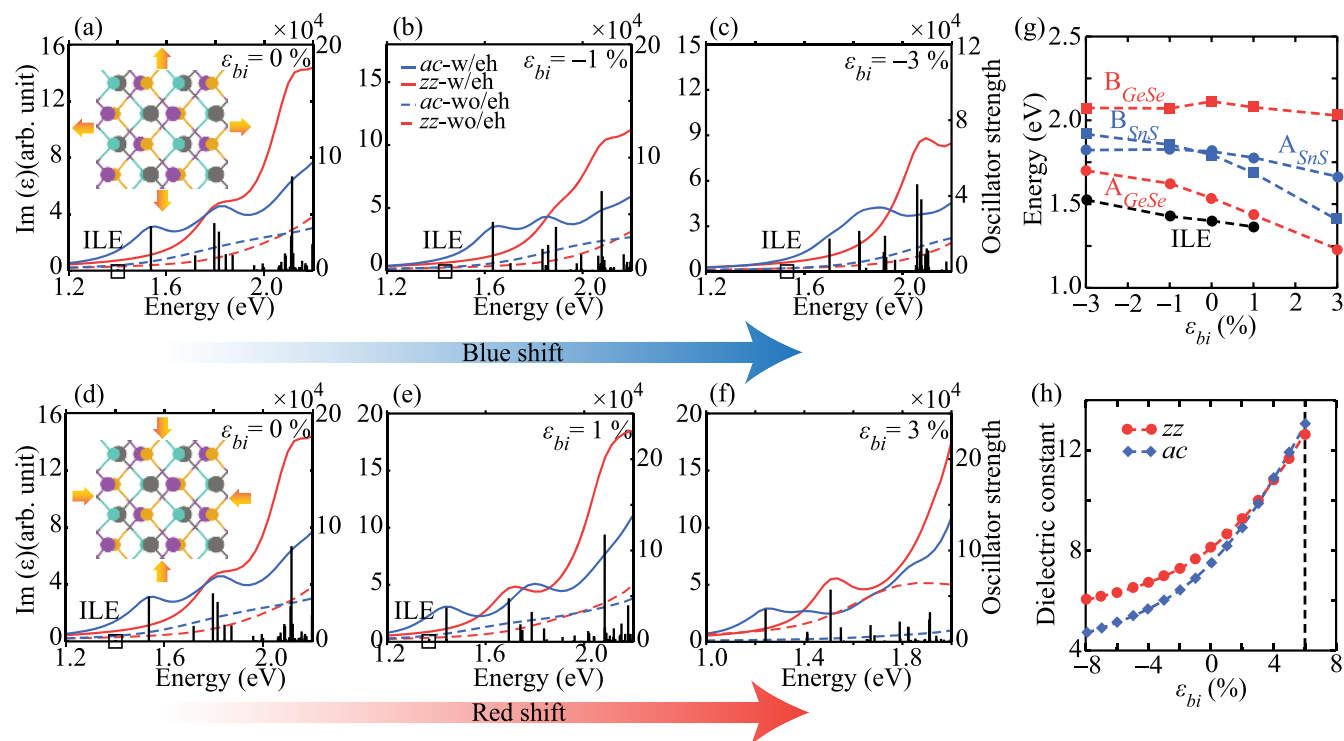


Figure 4. (a–c) Optical absorption spectra of GeSe/SnS heterostructure with bitensile (BT) strain. Optical absorption shows the blue shift. (d–f) Optical absorption spectra of GeSe/SnS heterostructure with bicompressive (BC) strain. Optical absorption shows the red shift. (g) Evolution of low-energy levels of intra- and interlayer excitonic states for different ϵ_{bi} . (h) Variation of static dielectric constants in the ac and zz directions as a function of ϵ_{bi} .

respect to the unstrained peak position as shown in Figure S11a–c (Figure S11d–f). The ILE is present throughout the whole out-of-plane strain (–3 to 3%) range. To understand the red and blue shift of optical absorption and excitonic energy levels with ϵ_{bi} the static dielectric constant for all the strain has been calculated as shown in Figure 4h. The BC strain brings atoms closer to each other and leads to greater overlap of the orbitals. It results in an increase of dielectric screening (ϵ) of the system (Figure 4h) in both ac and zz directions, and the absorption peaks corresponding to intra- and interlayer excitons show a blue shift with the BT strain and a red shift with the BC strain.

The E_{ex} values of intra- and interlayer exciton (except B_{GeSe}) remain almost constant with the external ϵ_{bi} as shown in Figure 5a. The variation of the excitonic energy levels (Figure 4g) and

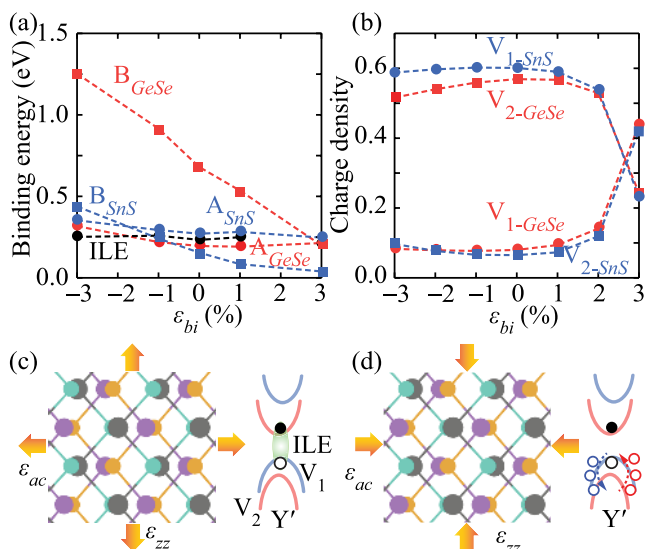


Figure 5. (a) Variation of binding energies of intra- and interlayer excitonic states for different ϵ_{bi} . (b) Evolution of electronic states of V_1 and V_2 valleys as a function of ϵ_{bi} . (c, d) Schematic representation of IL transition states at BT (–3%) and BC (2%) strains, respectively.

the corresponding electronic direct band gap (Figure S12) with respect to ϵ_{bi} follow the same trend (except B_{GeSe}). Therefore, the difference between the electronic direct band gap and excitonic energy level remains almost constant, leading to unaltered behavior of the excitonic binding energies. The small decrease in the excitonic binding energies can be understood by using the Mott–Wannier effective mass model. The two-body excitonic binding energy of an ideal 2D sheet^{42,43} in the Mott–Wannier effective model can be written as $E_{\text{ex}}^{2D} = \frac{54.4\mu_{\text{ex}}}{m_0\epsilon^2}$, where m_0 , $\mu_{\text{ex}} = m_e m_h / (m_e + m_h)$, and ϵ are the free electron mass, the effective mass of the exciton, and the static dielectric constant of the system, respectively. The excitonic binding energy of ILE calculated via the classical Mott–Wannier model was found to be closer (0.11 eV) to the BSE-calculated value (0.23 eV). With increasing dielectric screening, a decrease in binding energy of excitons is observed (Figure 5a). The variation of excitonic binding energies as a function of ϵ_{bi} is more noticeable in B excitons compared to that of the A excitons. Because of the greater overlap of electronic states along the zz direction for all the strains, the dielectric constant is higher along the zz direction compared to

the ac direction (Figure 4h). Compared to all the intralayer excitons, the variation in the binding energy of ILE is very small. Because of the localization of electrons and holes in different layers at Y' , the optical band gap (Figure 4g) follows exactly the same trend as that of the electronic band gap (Figure S12) at Y' , and as a result, the E_{ex} of ILE remains constant.

From Figures 4f,g and 5a, it is observed that the ILE disappears at higher compressive strain. In order to get the physical insight, the contributions of electronic states from different layers in V_1 and V_2 valleys for ϵ_{bi} have been calculated. The evolution of GeSe and SnS electronic states in V_1 and V_2 valleys with strain are shown in Figure 5b. It is observed that the major (minor) contributions of electronic states in V_1 and V_2 valleys are from SnS (GeSe) and GeSe (SnS) layers, respectively (Figure 5b). The application of ϵ_{bi} leads to charge transfer between these two valleys. The contribution of the electronic states from different layers in V_1 and V_2 valleys does not change much in the case of ϵ_{bi} from –3% to 1% as shown in Figure 5b. Therefore, the charge transfer between these two valleys is very small up to 1% biaxial strain, helping the heterostructure to preserve the type II alignment as well as the interlayer anisotropic exciton in this range of ϵ_{bi} (Figure 5c). Beyond 1% BC strain, the charge transfer between the layers becomes enormously high (Figure 5b), and both the valleys (V_1 and V_2) no longer act as isolated monolayer electronic states. At this ϵ_{bi} , the Y' does not remain type II, and as a result the interlayer excitonic bound state disappears (Figure 5d).

In summary, we have studied the generation of linearly polarized, anisotropic intra- and interlayer excitonic bound states in the GeSe/SnS van der Waals heterostructure. Our calculations suggest that the puckered 2D honeycomb-like geometry leads to directional anisotropy in excitonic bound state of this heterostructure. A variation in excitonic binding energies and optical band gap has been observed, which is ascribed to the change in effective dielectric constant and the band dispersion upon application of biaxial strain. The red/blue shift of the optical absorption spectrum is observed upon applying compressive/tensile biaxial strains. The destruction of type II band alignment and hence linearly polarized anisotropic ILE has also been found for the higher biaxial compressive strain due to the charge transfer between the layers. This study provides a useful guidance for the optimization of the excitonic binding energies and tuning the formation of interlayer excitonic bound state, which can assist its applications in photovoltaics, lasers, optical quantum computers, and optoelectronic devices.

■ ASSOCIATED CONTENT

Supporting Information

The Supporting Information is available free of charge at <https://pubs.acs.org/doi/10.1021/acs.jpcllett.0c03469>.

Details of ground state and quasi-particle energy calculations, convergence of ground state energy with respect to plane wave energy cutoff and k -mesh size of monolayers GeSe, SnS, and the GeSe/SnS vdW heterostructure, convergence of optical absorption and excitonic levels of the GeSe/SnS vdW heterostructure with respect to frequency grid, number of bands, and k -grid in GOW0-BSE calculations, optimized structures of monolayers GeSe, SnS, and AA and AB stacking of the

GeSe/SnS vdW heterostructure along with lattice parameters, phonon band structures of monolayers GeSe and SnS, comparison of optimized energies of AA and AB stacking of the GeSe/SnS vdW heterostructure with DFT-D2 and -D3 vdW functionals, interface energy of the GeSe/SnS vdW heterostructure, PBE and GW band structures of monolayers GeSe and SnS, calculated values of effective mass (m^*), elastic modulus (C), deformation potential (E), and mobility (μ) for electrons (e) and holes (h) in the ac and zz directions of monolayers GeSe, SnS, and GeSe/SnS vdW heterostructure, optical properties and excitonic energies of monolayers GeSe and SnS, static dielectric constants of monolayers and vdW heterostructure, optical properties of the GeSe/SnS vdW heterostructure under out-of-plane strain, variation of static dielectric constant and direct band gap of the GeSe/SnS vdW heterostructure under in-plane biaxial strain (PDF)

AUTHOR INFORMATION

Corresponding Author

Abhishek Kumar Singh – Materials Research Centre, Indian Institute of Science, Bangalore 560012, India; orcid.org/0000-0002-7631-6744; Email: abhishek@iisc.ac.in

Authors

Nikhilesh Maity – Materials Research Centre, Indian Institute of Science, Bangalore 560012, India

Pooja Srivastava – Amity School of Applied Sciences, Amity University Uttar Pradesh, Lucknow, Uttar Pradesh 226010, India

Himani Mishra – Materials Research Centre, Indian Institute of Science, Bangalore 560012, India

Ravindra Shinde – Materials Research Centre, Indian Institute of Science, Bangalore 560012, India; orcid.org/0000-0001-5182-1480

Complete contact information is available at:

<https://pubs.acs.org/10.1021/acs.jpcclett.0c03469>

Notes

The authors declare no competing financial interest.

ACKNOWLEDGMENTS

The authors acknowledge Ritesh Kumar for in-depth discussions. The authors thank Material Research Centre and Supercomputer Educational and Research Centre, Indian Institute of Science, Bangalore, for the computational facilities. This project has been supported by the India–Korea joint programme in Science and Technology. R.S. acknowledges the Science and Engineering Research Board, DST, India, for a fellowship (PDF/2015/000466). A.K.S. and P.S. acknowledge the support from Science and Engineering Research Board, DST Teachers Associateship for Research Excellence (TARE, TAR/2018/000834) program.

REFERENCES

- (1) Radisavljevic, B.; Radenovic, A.; Brivio, J.; Giacometti, V.; Kis, A. Single-Layer MoS₂ Transistors. *Nat. Nanotechnol.* **2011**, *6*, 147–150.
- (2) Wang, Q. H.; Kalantar Zadeh, K.; Kis, A.; Coleman, J. N.; Strano, M. S. Electronics and Optoelectronics of Two-dimensional Transition Metal Dichalcogenides. *Nat. Nanotechnol.* **2012**, *7*, 699–712.

- (3) Kim, J.; Jin, C.; Chen, B.; Cai, H.; Zhao, T.; Lee, P.; Kahn, S.; Watanabe, K.; Taniguchi, T.; Tongay, S.; et al. Observation of Ultralong Valley Lifetime in WSe₂/MoS₂ Heterostructures. *Sci. Adv.* **2017**, *3*, No. e1700518.

- (4) Hsu, W.-T.; Lu, L.-S.; Wu, P.-H.; Lee, M.-H.; Chen, P.-J.; Wu, P.-Y.; Chou, Y.-C.; Jeng, H.-T.; Li, L.-J.; Chu, M.-W.; Chang, W.-H. Negative Circular Polarization Emissions from WSe₂/MoSe₂ Commensurate Heterobilayers. *Nat. Commun.* **2018**, *9*, 1356.

- (5) Eda, G.; Maier, S. A. Two-Dimensional Crystals: Managing Light for Optoelectronics. *ACS Nano* **2013**, *7*, 5660–5665.

- (6) Xia, F.; Wang, H.; Xiao, D.; Dubey, M.; Ramasubramanian, A. Two-Dimensional Material Nanophotonics. *Nat. Photonics* **2014**, *8*, 899–907.

- (7) Yu, Y.; Hu, S.; Su, L.; Huang, L.; Liu, Y.; Jin, Z.; Puzosky, A. A.; Geohagan, D. B.; Kim, K. W.; Zhang, Y.; et al. Equally Efficient Interlayer Exciton Relaxation and Improved Absorption in Epitaxial and Nonepitaxial MoS₂/WS₂ Heterostructures. *Nano Lett.* **2015**, *15*, 486–491.

- (8) Geim, A. K.; Grigorieva, I. V. Van der Waals Heterostructures. *Nature* **2013**, *499*, 419–425.

- (9) Bernardi, M.; Palumbo, M.; Grossman, J. C. Extraordinary Sunlight Absorption and One Nanometer Thick Photovoltaics Using Two-Dimensional Monolayer Materials. *Nano Lett.* **2013**, *13*, 3664–3670.

- (10) Hong, X.; Kim, J.; Shi, S. F.; Zhang, Y.; Jin, C.; Sun, Y.; Tongay, S.; Wu, J.; Zhang, Y.; Wang, F. Ultrafast Charge Transfer in Atomically Thin MoS₂/WS₂ Heterostructures. *Nat. Nanotechnol.* **2014**, *9*, 682–686.

- (11) Komsa, H. P.; Krasheninnikov, A. V. Electronic Structures and Optical Properties of Realistic Transition Metal Dichalcogenide Heterostructures from First Principles. *Phys. Rev. B: Condens. Matter Mater. Phys.* **2013**, *88*, 085318.

- (12) Singh, A.; Manjanath, A.; Singh, A. K. Engineering Defect Transition-Levels through the van der Waals Heterostructure. *J. Phys. Chem. C* **2018**, *122*, 24475–24480.

- (13) Kumar, R.; Das, D.; Singh, A. K. C₂N/WS₂ van der Waals Type-II Heterostructure as a Promising Water Splitting Photocatalyst. *J. Catal.* **2018**, *359*, 143–150.

- (14) Britnell, L.; Gorbachev, R. V.; Jalil, R.; Belle, B. D.; Schedin, F.; Mishchenko, A.; Georgiou, T.; Katsnelson, M. I.; Eaves, L.; Morozov, S. V.; et al. Field-Effect Tunneling Transistor Based on Vertical Graphene Heterostructures. *Science* **2012**, *335*, 947–950.

- (15) Rivera, P.; Schaibley, J. R.; Jones, A. M.; Ross, J. S.; Wu, S.; Aivazian, G.; Klement, P.; Seyler, K.; Clark, G.; Ghimire, N. J.; et al. Observation of Long-Lived Interlayer Excitons in Monolayer MoSe₂-WSe₂ Heterostructures. *Nat. Commun.* **2015**, *6*, 6242.

- (16) Latini, S.; Winther, K. T.; Olsen, T.; Thygesen, K. S. Interlayer Excitons and Band Alignment in MoS₂/hBN/WSe₂ van der Waals Heterostructures. *Nano Lett.* **2017**, *17*, 938–945.

- (17) Zhang, C.; Jiao, Y.; He, T.; Bottle, S.; Frauenheim, T.; Du, A. Predicting Two-Dimensional C₃B/C₃N van der Waals p-n Heterojunction with Strong Interlayer Electron Coupling and Enhanced Photocurrent. *J. Phys. Chem. Lett.* **2018**, *9*, 858–862.

- (18) Deilmann, T.; Thygesen, K. S. Interlayer Trions in the MoS₂/WS₂ van der Waals Heterostructure. *Nano Lett.* **2018**, *18*, 1460–1465.

- (19) Fogler, M. M.; Butov, L. V.; Novoselov, K. S. High-Temperature Superfluidity with Indirect Excitons in van der Waals Heterostructures. *Nat. Commun.* **2014**, *5*, 4555.

- (20) Furchi, M. M.; Pospischil, A.; Libisch, F.; Burgdörfer, J.; Mueller, T. Photovoltaic Effect in an Electrically Tunable van der Waals Heterojunction. *Nano Lett.* **2014**, *14*, 4785–4791.

- (21) Xue, Y.; Zhang, Y.; Liu, Y.; Liu, H.; Song, J.; Sophia, J.; Liu, J.; Xu, Z.; Xu, Q.; Wang, Z.; et al. Scalable Production of a Few-Layer MoS₂/WS₂ Vertical Heterojunction Array and Its Application for Photodetectors. *ACS Nano* **2016**, *10*, 573–580.

- (22) Wang, X.; Jones, A. M.; Seyler, K. L.; Tran, V.; Jia, Y.; Zhao, H.; Wang, H.; Yang, L.; Xu, X.; Xia, F. Highly Anisotropic and Robust Excitons in Monolayer Black Phosphorus. *Nat. Nanotechnol.* **2015**, *10*, 517.

- (23) Echeverry, J. P.; Gerber, I. C. Theoretical Investigations of the Anisotropic Optical Properties of Distorted 1TReS₂ and ReSe₂ Monolayers, Bilayers, and in the Bulk Limit. *Phys. Rev. B: Condens. Matter Mater. Phys.* **2018**, *97*, 075123.
- (24) Zhou, Y.; Maity, N.; Rai, A.; Juneja, R.; Meng, X.; Roy, A.; Zhang, Y.; Xu, X.; Lin, J. F.; Banerjee, S. K.; et al. Stacking-Order-Driven Optical Properties and Carrier Dynamics in ReS₂. *Adv. Mater.* **2020**, *32*, 1908311.
- (25) Xu, L.; Yang, M.; Wang, S. J.; Feng, Y. P. Electronic and Optical Properties of the Monolayer Group-IV Monochalcogenides MX (M = Ge, Sn; X = S, Se, Te). *Phys. Rev. B: Condens. Matter Mater. Phys.* **2017**, *95*, 235434.
- (26) Gomes, L. C.; Trevisanutto, P. E.; Carvalho, A.; Rodin, A. S.; Castro Neto, A. H. Strongly Bound Mott-Wannier Excitons in GeS and GeSe Monolayers. *Phys. Rev. B: Condens. Matter Mater. Phys.* **2016**, *94*, 155428.
- (27) Xu, Y.; Zhang, H.; Shao, H.; Ni, G.; Li, J.; Lu, H.; Zhang, R.; Peng, B.; Zhu, Y.; Zhu, H.; et al. First-principles Study on the Electronic, Optical, and Transport Properties of Monolayer α - and β -GeSe. *Phys. Rev. B: Condens. Matter Mater. Phys.* **2017**, *96*, 245421.
- (28) Hu, Z. Y.; Li, K. Y.; Lu, Y.; Huang, Y.; Shao, X. H. High Thermoelectric Performances of Monolayer SnSe Allotropes. *Nanoscale* **2017**, *9*, 16093–16100.
- (29) Huang, Z.; Zhang, W.; Zhang, W. Computational Search for Two-Dimensional MX₂ Semiconductors with Possible High Electron Mobility at Room Temperature. *Materials* **2016**, *9*, 716.
- (30) Qiao, J.; Kong, X.; Hu, Z. X.; Yang, F.; Ji, W. High-Mobility Transport Anisotropy and Linear Dichroism in Few-Layer Black Phosphorus. *Nat. Commun.* **2014**, *5*, 4475.
- (31) Knill, E.; Laflamme, R.; Milburn, G. J. A Scheme for Efficient Quantum Computation with Linear Optics. *Nature* **2001**, *409*, 46–52.
- (32) Nan, Z.; Xiaoyu, J.; Qiang, G.; Yonghong, H.; Hui, M. Linear Polarization Difference Imaging and Its Potential Applications. *Appl. Opt.* **2009**, *48*, 6734–6739.
- (33) Nayak, A. P.; Bhattacharyya, S.; Zhu, J.; Liu, J.; Wu, X.; Pandey, T.; Jin, C.; Singh, A. K.; Akinwande, D.; Lin, J. F. Pressure-Induced Semiconducting to Metallic Transition in Multilayered Molybdenum Disulfide. *Nat. Commun.* **2014**, *5*, 3731.
- (34) He, K.; Poole, C.; Mak, K. F.; Shan, J. Experimental Demonstration of Continuous Electronic Structure Tuning via Strain in Atomically Thin MoS₂. *Nano Lett.* **2013**, *13*, 2931–2936.
- (35) Kim, J. S.; Ahmad, R.; Pandey, T.; Rai, A.; Feng, S.; Yang, J.; Lin, Z.; Terrones, M.; Banerjee, S. K.; Singh, A. K.; et al. Towards Band Structure and Band Offset Engineering of Monolayer Mo_(1-x)W_(x)S₂ via Strain. *2D Mater.* **2018**, *5*, 015008.
- (36) Su, J.; He, J.; Zhang, J.; Lin, Z.; Chang, J.; Zhang, J.; Hao, Y. Unusual Properties and Potential Applications of Strain BN-MS₂ (M = Mo, W) Heterostructures. *Sci. Rep.* **2019**, *9*, 3518.
- (37) Nayak, A. P.; Pandey, T.; Voiry, D.; Liu, J.; Moran, S. T.; Sharma, A.; Tan, C.; Chen, C. H.; Li, L. J.; Chhowalla, M.; et al. Pressure-Dependent Optical and Vibrational Properties of Monolayer Molybdenum Disulfide. *Nano Lett.* **2015**, *15*, 346–353.
- (38) Zhang, Q.; Chang, Z.; Xu, G.; Wang, Z.; Zhang, Y.; Xu, Z. Q.; Chen, S.; Bao, Q.; Liu, J. Z.; Mai, Y. W.; et al. Strain Relaxation of Monolayer WS₂ on Plastic Substrate. *Adv. Funct. Mater.* **2016**, *26*, 8707–8714.
- (39) Bertolazzi, S.; Brivio, J.; Kis, A. Stretching and Breaking of Ultrathin MoS₂. *ACS Nano* **2011**, *5*, 9703–9709.
- (40) Xia, J.; Yan, J.; Wang, Z.; He, Y.; Gong, Y.; Chen, W.; Sum, T. C.; Liu, Z.; Ajayan, P. M.; Shen, Z. Strong Coupling and Pressure Engineering in WSe₂-MoSe₂ Heterobilayers. *Nat. Phys.* **2020**.
- (41) Çakır, D.; Sahin, H.; Peeters, F. M. Tuning of the Electronic and Optical Properties of Single-Layer Black Phosphorus by Strain. *Phys. Rev. B: Condens. Matter Mater. Phys.* **2014**, *90*, 205421.
- (42) Ramasubramanian, A. Large Excitonic Effects in Monolayers of Molybdenum and Tungsten Dichalcogenides. *Phys. Rev. B: Condens. Matter Mater. Phys.* **2012**, *86*, 115409.
- (43) Cheiwchanchamnangij, T.; Lambrecht, W. R. L. Quasiparticle Band Structure Calculation of Monolayer, Bilayer, and Bulk MoS₂. *Phys. Rev. B: Condens. Matter Mater. Phys.* **2012**, *85*, 205302.